AIAA 2004–2636

DSMC Calculations of Rarefied Hypersonic Flow over Power Law Leading Edges with Incomplete Surface Accommodation

Wilson F. N. Santos
National Institute for Space Research
Cachoeira Paulista, SP 12630–000 BRAZIL

Mark J. Lewis
University of Maryland, College Park, MD 20742

34th AIAA Fluid Dynamics Conference and Exhibit
28 June–1 July, 2004/Portland, OR

DSMC Calculations of Rarefied Hypersonic Flow over Power Law Leading Edges with Incomplete Surface Accommodation

Wilson F. N. Santos*
National Institute for Space Research
Cachoeira Paulista, SP 12630–000 BRAZIL

Mark J. Lewis†
University of Maryland, College Park, MD 20742

This work describes a computational study on hypersonic flow past power law shaped leading edges at zero incidence. Effects of incomplete surface accommodation in rarefied flow on the aerothermodynamic surface quantities have been investigated by employing the Direct Simulation Monte Carlo Method in combination with the Cercignani-Lampis-Lord gas surface interaction model, which incorporates separate accommodation coefficients for the normal and tangential velocity components. The work is motivated by interest in assessing the overall performance of power-law shaped leading edges in order to consider them as possible candidates for blunting geometries of hypersonic leading edges. The results presented highlight the sensitivity of the heat transfer and drag coefficients to changes on the gas-surface accommodation coefficients. It was found that the heat transfer coefficient diminishes with decreasing the normal accommodation coefficient, and increases slightly by a reduction in the tangential accommodation coefficient in the vicinity of the stagnation region.

Nomenclature

a	Constant in power-law body equation
C_d	Drag coefficient, Eq. (11)
C_h	Heat transfer coefficient, Eq. (5)
c	Molecular velocity, m/s
D	Drag force, N
e	specific energy, J/kg
H	Body height at the base, m
Kn	Knudsen number
L	Body length, m
M	Mach number
m	Molecular mass, kg
N	Number of molecules
n	Body power law exponent
p	Pressure, N/m^2
q	Heat flux, W/m^2
Re	Reynolds number
s	Arc length, m
T	Temperature, K
V	Velocity, m/s
x, y	Cartesian axes in physical space, m
α	Thermal accommodation coefficient
η	Coordinate normal to body surface, m
θ	Wedge half angle, body slope angle, deg
Θ	Angle of incidence or reflection, deg
λ	Mean free path, m
ξ	Coordinate tangent to body surface, m
ρ	Density, kg/m^3
σ	Momentum accommodation coefficient
τ	Shear stress, N/m^2

Subscripts

n	Normal
R	Rotational
t	Tangential
V	Vibrational
w	Wall conditions
∞	Freestream conditions

Introduction

AN increasingly important problem in aerospace engineering is that of predicting aerodynamic characteristics of vehicles flying at very high speeds and high altitudes. Under this conditions, the flow about a given aerodynamic configuration may be sufficiently rarefied that the appropriate mean free path becomes too large, compared to a characteristic length of the vehicle, for the use of continuum assumptions but not large enough for the use of the free molecular theory. In such an intermediate or transition rarefied gas regime, the complete investigation of the flowfield structure would require the full formulation of kinetic theory. The governing equation in the transition regime is the Boltzmann equation[1]. Nevertheless, in order to circumvent the difficult of a direct solution of the Boltzmann equation, the Direct Simulation

*Researcher, Combustion and Propulsion Laboratory. AIAA Member.

†Professor, Aerospace Engineering Department. AIAA Associate Fellow.

Monte Carlo (DSMC) method[2] has been the appropriate choice for problems involving flows of rarefied hypersonic aerothermodynamics.

One of the key issues concerning hypersonic configurations is the leading edge of the vehicle. Hypersonic configurations are generally characterized by slender bodies and sharp leading edges in order to achieve good aerodynamic properties like high lift and low drag. Nevertheless, for flight at hypersonic speeds, the vehicle leading edges must be sufficiently blunt in order to reduce the heat transfer rate to acceptable levels, and possibly to allow for internal heat conduction. In this context, power law shaped leading edges ($y \propto x^n, 0 < n < 1$) have been considered as especially promising bluntness for hypersonic configurations in order to provide the leading edge heating and manufacturing requirements. This concept is based on the work of Mason and Lee[3], who have pointed out that, for certain exponents, power law shapes exhibit both blunt (infinite body slope at the nose) and sharp (zero radius of curvature at the nose) characteristics.

A great deal of works[4−10] has been carried out recently on power-law form representing blunt geometries. The major interest in these works has gone into considering the power-law shape as possible candidates for blunting geometries of hypersonic leading edges, such as hypersonic waverider vehicles[11] which have been lately considered for high-altitude/low-density applications[12−15].

These works[5−10] on hypersonic flow past power-law shapes have been concentrated primarily on the analysis of the aerothermodynamic surface quantities by considering the diffuse reflection model as being the gas-surface interaction. The diffuse model assumes that the molecules are reflected equally in all directions, quite independently of their incident speed and direction. As a space flight vehicle is exposed to a rarefied environment over a considerable time, a departure from the fully diffuse model is observed, resulting from the colliding molecules that clean the surface of the vehicle, which becomes gradually decontaminated. Molecules reflected from clean surfaces show lobular distribution in direction. The flux distribution of scattered molecules emitted from clean surfaces frequently has a lobular shape that is centered about an angle which tends to approach the specular angle for very high energies and/or low angle of attack.

Both the aerodynamic surface quantities and the state of the gas adjacent to the body surface are very sensitive to the assumptions used in the calculation concerning the gas-surface interaction model for transitional and free molecular flows. In addition, the essential phenomena of rarefied gases are found mostly in the region relatively near to the solid boundaries, i.e., within a few mean free paths. Thus a knowledge of the physics of the interaction of gas molecules and solid surfaces is of primary importance.

In an effort to obtain further insight into the nature of the flowfield structure of power law leading edges under hypersonic transitional flow conditions, a parametric study is performed on these shapes with a great deal of emphasis placed on the gas-surface interaction effects. In this scenario, the primary goal of this paper is to assess the sensitivity of the aerothermodynamic surface quantities to variations in the surface accommodation coefficients experienced by the leading edges by employing the Cercignani-Lampis-Lord (CLL) model[16]. The CLL model, which incorporates independent accommodation coefficients for the normal and tangential velocity components, is implemented into the DSMC code, and simulations are performed by assuming two-dimensional rarefied hypersonic flow.

Gas-Surface Interaction Model

The influence of the model of gas-surface interactions on the aerodynamic forces and heat transfer increases substantially as the gas rarefaction increases. As a result, a correct choice of the model for calculating hypersonic rarefied flows plays an important role.

Three models of gas-surface interactions may be employed in the DSMC method: specular and diffuse interactions and some combination of these. In a specular reflection, molecules are reflected like a perfectly elastic sphere with reversal of the normal component of velocity and no change in either the parallel components of velocities and energy. In a diffuse reflection, the molecules are reflected equally in all directions, and the final velocity of the molecules is randomly assigned according to a half-range Maxwellian distribution determined by the wall temperature. The combination of diffuse reflection with specular reflection (Maxwell model) introduces a single parameter f to indicate the fraction of those molecules reflected diffusely in a completely accommodated fashion according to a Maxwellian distribution corresponding to the wall temperature, and the remaining fraction (1-f), being assumed to reflect specularly.

The Maxwell model was followed by the introduction of three accommodation coefficients that describe the degree of accommodation of the incident normal momentum, tangential momentum and kinetic energy to those of the surface. The traditional definition[17] for these coefficients are usually expressed as being,

$$\sigma_n = \frac{p_i - p_r}{p_i - p_w} \quad (1)$$

$$\sigma_t = \frac{\tau_i - \tau_r}{\tau_i} \quad (2)$$

$$\alpha = \frac{e_i - e_r}{e_i - e_w} \quad (3)$$

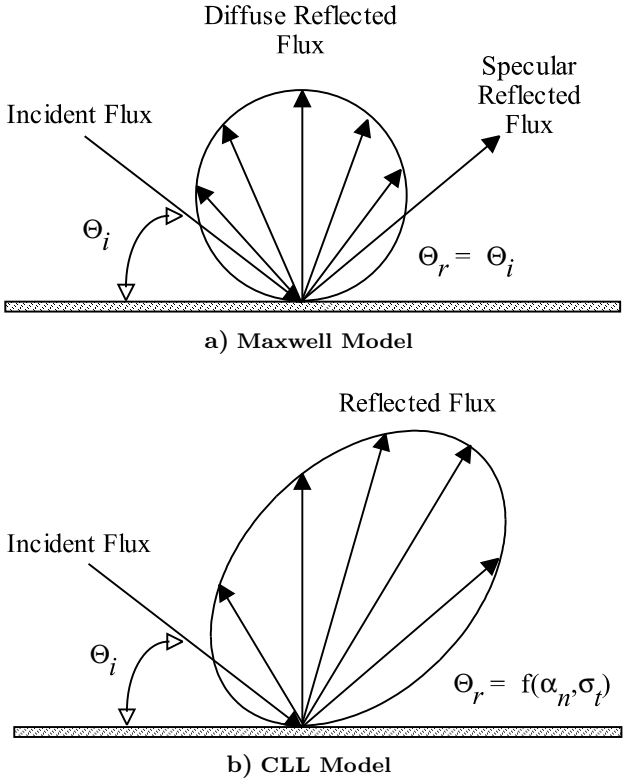

Fig. 1 Drawing illustrating the Maxwell reflection model and the CLL reflection model.

where terms p, τ and e refer to the momentum flux acting normal and tangential to the surface, and the energy flux to the surface per unit area per unit time, respectively; subscripts i and r stand for the incident and reflected components, and w refers to the component that would be produced by a diffuse reflection at the temperature of the surface.

Data from many experiments show that molecules reflected or re-emitted from solid surfaces present lobular distributions under high vacuum conditions and are poorly represented by the Maxwell model. However, this model is widely used because it satisfies the principle of detailed balance or reciprocity. Detailed balance means that at equilibrium every molecular process and its inverse process must individually balance.

A phenomenological model that satisfies detailed balance and has demonstrated improvement over the Maxwell model has been proposed by Cercignani and Lampis[18] (CL model). This model is based on the definition of the accommodation coefficients α_n and α_t that represent the accommodation coefficients for the kinetic energy associated with the normal and tangential components of velocity. The CL model provides a continuous spectrum of behavior from specular reflection at one end to diffuse reflection with complete energy accommodation at the other, and produces physically realistic distributions of direction and energy re-emitted molecules. Lord[16] has shown that the CL model is suited for the DSMC method, and described how to incorporate it into the DSMC method. The DSMC method with Lord's implementation is referred as the Cercignani-Lampis-Lord (CLL) method. The CLL model is derived assuming that there is no coupling between the normal and tangential momentum components. The two adjustable parameters appearing in the CLL model are the normal component of translational energy α_n and the tangential component of momentum σ_t. Figure 1 displays a schematic comparison of the Maxwell reflection model and the CLL reflection model. The CL model has also been extended for covering diffuse scattering with partial energy accommodation and for simulating the accommodation of vibrational energy of a diatomic molecule modeled as simple harmonic oscillator[19] and an anharmonic oscillator[20].

In order to simulate the partial surface accommodation, the Cercignani-Lampis-Lord (CLL) model[16] was implemented in this DSMC calculation. However, in the implementation of the CLL model in the DSMC method, Bird[2] has shown that it is equivalent to specify the normal α_n and tangential α_t components of translational energy, since $\alpha_t = \sigma_t(2 - \sigma_t)$, and thus that $\sigma_t < \alpha_t$, assuming that σ_t lies between 0 and 1. In the present simulations, α_n and σ_t are used as being the two adjustable parameters. It is important to mention that in the CLL model the accommodation of internal energy is allowed to be independent of the translational accommodation.

Leading Edge Geometry Definition

In dimensional form, the body power law shapes are given by the following expression,

$$y = ax^n \tag{4}$$

where n is the power law exponent and a is the power law constant which is a function of n.

The power-law shapes are modeled by assuming a sharp leading edge of half angle θ with a circular cylinder of radius R inscribed tangent to this wedge. The power law shapes, inscribed between the wedge and the cylinder, are also tangent to both shapes at the same common point where they have the same slope angle. The circular cylinder diameter provides a reference for the amount of blunting desired on the leading edges. It was assumed a leading edge half angle of 10 deg, a circular cylinder diameter of 10^{-2}m and power law exponents of 1/2, 2/3 and 3/4. Figure 2 shows schematically this construction.

From geometric considerations, the power law constant a is obtained by matching slope on the wedge, circular cylinder and power law body at the tangency point. The common body height H at the tangency point is equal to $2R\cos\theta$, and the body length L from the nose to the tangency point in the axis of symmetry is given by $nH/2\tan\theta$. Since the wake region behind the power law bodies is not of interest in this investi-

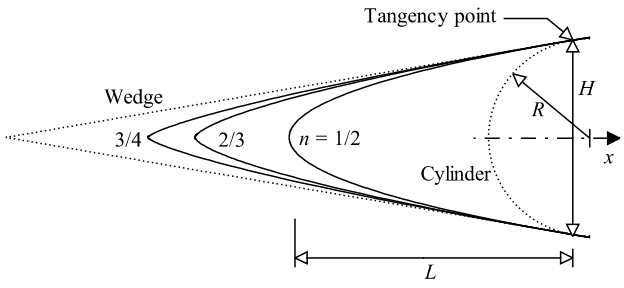

Fig. 2 Drawing illustrating the leading edge geometries.

gation, it was assumed that the power law bodies are infinitely long but only the length L is considered.

Computational Method and Procedure

It is well known that neither the continuum flow equations nor the collisionless flow equations are valid to predict leading edge aerothermodynamic characteristics throughout the transitional flow regime. During the last several years, the most successful numerical technique applied for computing leading edge flowfield and surface effects in the transitional flow regime has been the DSMC method pioneered by Bird[2].

The DSMC method simulates real gas flows with various physical processes by means of a huge number of modeling particles, each of which is a typical representative of great number of real gas molecules. DSMC models the flow as being a collection of discrete particles, each one with a position, velocity and internal energy. The state of particles is stored and modified with time as the particles move, collide, and undergo boundary interactions in simulated physical space.

The molecular collision kinetics are modeled using the variable hard sphere (VHS) molecular model[21] and the no time counter (NTC) collision sampling technique[22]. The energy exchange between kinetic and internal modes is controlled by the Borgnakke-Larsen statistical model[23]. Simulations are performed using a non-reacting gas model consisting of two chemical species, N_2 and O_2. Energy exchanges between the translational and internal modes are considered. For a given collision, the probabilities are designated by the inverse of the relaxation numbers, which correspond to the number of collisions necessary, on average, for a molecule to relax. For this study, the relaxation numbers of 5 and 50 were used for the rotation and vibration, respectively. The effective number of degrees of freedom in the partially excited vibrational states is calculated from the harmonic oscillator theory[2].

In order to implement the particle-particle collisions, the flowfield is divided into a number of regions, which are subdivided into computational cells. The cell provides a convenient reference for the sampling of the macroscopic gas properties. The dimensions of the cells must be such that the change in flow properties across each cell is small. The linear dimensions of the cells should be small in comparison with the scale length of the macroscopic flow gradients normal to the streamwise directions, which means that the cell dimensions should be of the order of the local mean free path or even smaller[24−25]. The cells are further subdivided into 4 subcells, 2 subcells/cell in each direction. The collision partners are selected from the same subcell for the establishment of the collision rate. Consequently, the flow resolution is much higher than the cell resolution. Time is advanced in discrete steps such that each step ought to be sufficiently small in comparison with the local mean collision time[26−27].

The computational domain used for the calculation is made large enough so that body disturbances do not reach the upstream and side boundaries, where freestream conditions are specified. A schematic view of the computational domain is depicted in Fig. 3. Advantage of the flow symmetry is taken into account, and molecular simulation is applied to one-half of a full configuration. Side I is defined by the body surface. Reflection with incomplete surface accommodation is the condition applied to this side. Side II is a plane of symmetry. In such a boundary, all flow gradients normal to the plane are zero. At the molecular level, this plane is equivalent to a specular reflecting boundary. Side III is the freestream side through which simulated molecules enter and exit. Finally, the flow at the downstream outflow boundary, side IV, is predominantly supersonic and vacuum condition is specified[2]. At this boundary, simulated molecules can only exit.

Numerical accuracy in DSMC method depends on the grid resolution chosen as well as the number of particles per computational cell. Both effects were investigated to determine the number of cells and the number of particles required to achieve grid independence solutions for the thermal nonequilibrium flow that arises near the nose of the leading edges. A discussion of both effects on the aerodynamic surface

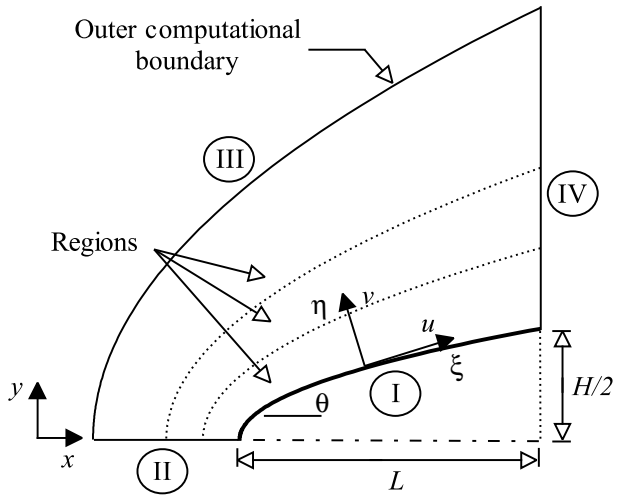

Fig. 3 Schematic view of the computational domain.

quantities for the set of power law shapes presented here is described in details in Ref. 10.

Flow Conditions

The freestream and flow conditions used for the numerical simulation of flow past the leading edges are those given by Santos[5] and summarized in Table 1, and the gas properties[2] are shown in Table 2.

The freestream velocity V_∞ is assumed to be constant at 3.5 km/s, which corresponds to freestream Mach number M_∞ of 12. The overall Knudsen number is defined as the ratio of the molecular mean free path in the freestream gas to a characteristic dimension of the flowfield. In the present study, the characteristic dimension was defined as being the diameter of the circular cylinder. Hence, the freestream Knudsen number Kn_∞ corresponds to 0.0903. The freestream Reynolds number by unit meter Re_∞ is 21455 based on conditions in the undisturbed stream. The translational and vibrational temperatures in the freestream are in equilibrium at 220 K, and the leading edge surface has a constant wall temperature T_w of 880 K for all cases considered.

In order to simulate the incomplete surface accommodation, the CLL model implemented in the DSMC code considered only the normal and tangential accommodation coefficients. The internal energy accommodation was kept equal to one for all calculations presented in this work. Hence, α_n and σ_t are used as being the two adjustable parameter. The DSMC calculations were performed independently for three distinct numerical values for α_n and σ_t: 0.6, 0.8 and 1.0. α_n and σ_t equal to 1.0 represents the diffusion reflection.

Table 1 Freestream and flow conditions

Parameter	Value	Unit
Altitude	70	km
Temperature (T_∞)	220.0	K
Pressure (p_∞)	5.582	N/m^2
Density (ρ_∞)	8.753×10^{-5}	kg/m^3
Viscosity (μ_∞)	1.455×10^{-5}	Ns/m^2
Number density (n_∞)	1.8209×10^{21}	m^{-3}
Mean free path (λ_∞)	9.03×10^{-4}	m

Table 2 Gas properties

Parameter	O_2	N_2	Unit
Molecular mass	5.312×10^{-26}	4.65×10^{-26}	kg
Molecular diameter	4.010×10^{-10}	4.11×10^{-10}	m
Mole fraction	0.237	0.763	
Viscosity index	0.77	0.74	

Computational Results and Discussion

Attention is now focused on the calculations of the surface aerodynamic quantities obtained from the DSMC results. The surface quantities of particular interest in the transition flow regime are the number flux, heat transfer, pressure, skin friction and drag. The purpose of this section is to discuss and to compare differences in the profiles of these properties, expressed in coefficient form, due to variations on the normal and tangential accommodation coefficients associated to the gas-surface interaction.

Number Flux

The number flux N is calculated by sampling the molecules impinging on the surface by unit time and unit area. The dependence of the number flux on the normal accommodation coefficient α_n is shown in Fig. 4 for power law exponents of 1/2, 2/3 and 3/4. In this set of plots, N^* is the number flux N normalized by $n_\infty V_\infty$, and S is the arc length s normalized by the freestream mean free path λ_∞. According to these plots, the number flux is very sensitive to changes in the normal accommodation coefficient provided that the leading edge is blunt. It is seen that the number flux decreases with decreasing the normal accommodation coefficient. In contrast, as the leading edge becomes aerodynamically sharp[3], $n > 2/3$, virtually no effect can be detected in the number flux.

Figure 5 illustrates the differences in the number flux due to variations in the tangential accommodation coefficient σ_t for the same set of leading edges. This set of plots exhibits essentially the same qualitative behavior when compared to that presented by changes in the normal accommodation coefficient α_n, i.e., the number flux diminishes for the power law shapes investigated. Nevertheless, the manner in which the number flux is reduced by changes in the two accommodation coefficients differs from blunt to aerodynamically sharp leading edges. Blunt leading edges are more affected by the normal accommodation coefficient whereas sharp leading edges are more affected by tangential accommodation coefficient.

Heat Transfer Coefficient

The heat transfer coefficient C_h is defined as follows,

$$C_h = \frac{q_w}{\rho_\infty V_\infty^3/2} \tag{5}$$

where the heat flux q_w to the body surface is calculated by the net energy flux of the molecules impinging on the surface. A flux is regarded as positive if it is directed toward the body surface. The net heat flux q_w is related to the sum of the translational, rotational and vibrational energies of both incident and reflected molecules as defined by,

$$q_w = q_i + q_r = \sum_{j=1}^{N} [\frac{1}{2} m_j c_j^2 + e_{Rj} + e_{Vj}]_i \ +$$

$$\sum_{j=1}^{N}[\frac{1}{2}m_j c_j^2 + e_{Rj} + e_{Vj}]_r \qquad (6)$$

where N is the number of molecules colliding with the surface by unit time and unit area, m is the mass of the molecules, c is the velocity of the molecules, e_R and e_V stand for the rotational and vibrational energies,

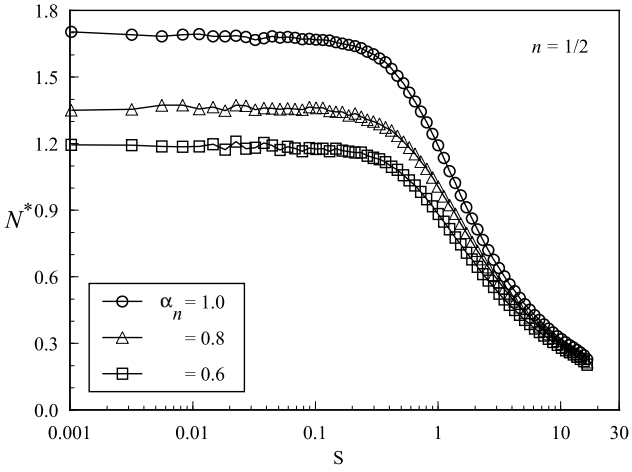

a) $n = 1/2$ **body shape**

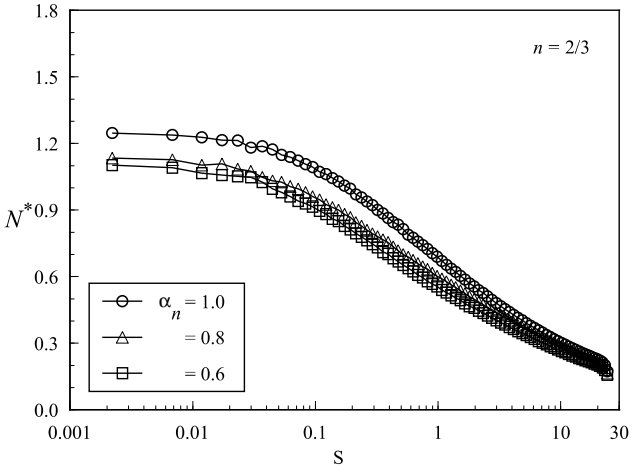

b) $n = 2/3$ **body shape**

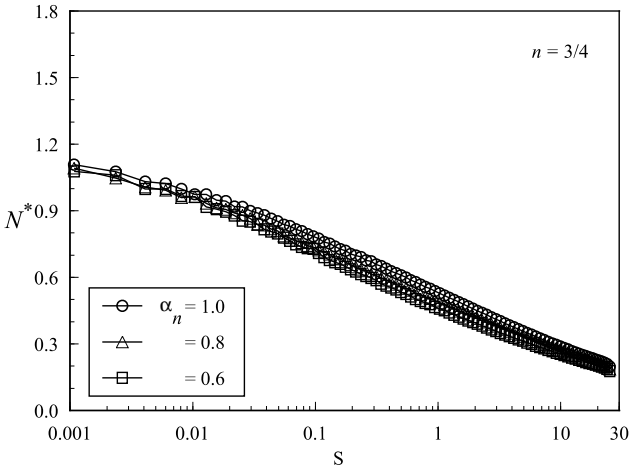

c) $n = 3/4$ **body shape**

Fig. 4 Effect of normal accommodation coefficient α_n on number flux along the body surface.

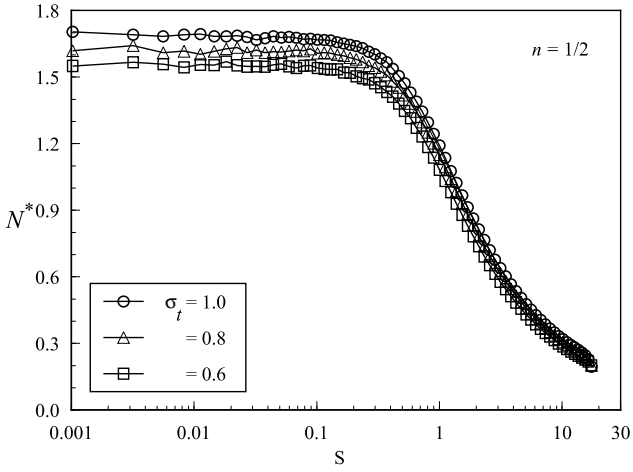

a) $n = 1/2$ **body shape**

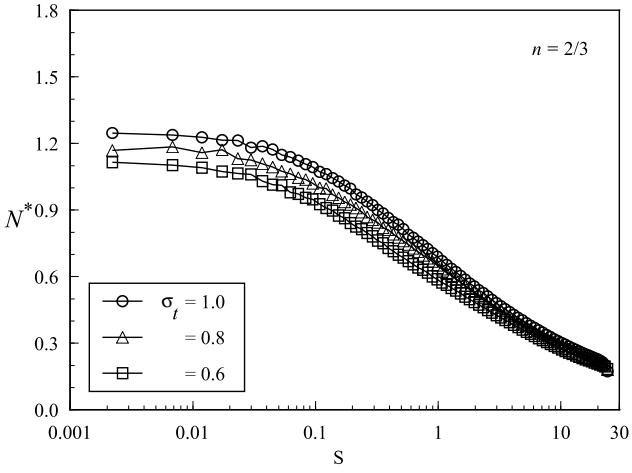

b) $n = 2/3$ **body shape**

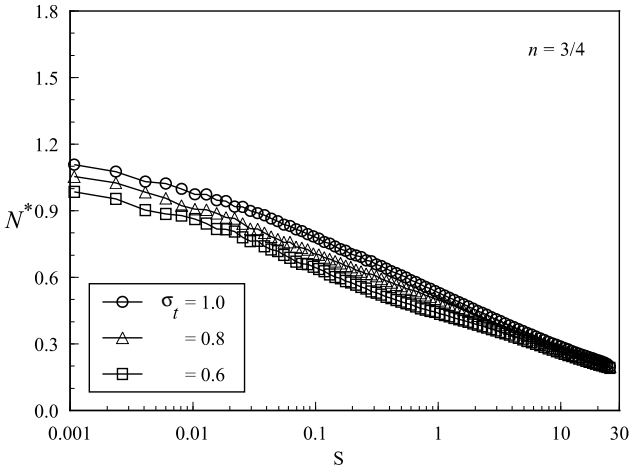

c) $n = 3/4$ **body shape**

Fig. 5 Effect of tangential accommodation coefficient σ_t on number flux along the body surface.

respectively. Subscripts i and r refer to incident and reflect molecules.

The effect of changing the normal accommodation coefficient α_n on the heat transfer coefficient C_h is plotted in Fig. 6 as a function of the dimensionless arc length S. According to these plots, it is seen that the net heat transfer coefficient decreases with decreasing α_n for the power law shapes investigated. An understanding of this behavior can be gained by considering independently the contribution of the incident q_i and reflected q_r heat fluxes that appear in Eq.(6). It is found[5] that the incident heat flux is almost identical as the normal accommodation coefficient α_n changes from 1.0 to 0.6. Nevertheless, the reflected heat flux increases drastically for the same range of α_n in the vicinity of the stagnation region of the leading edges. This effect is more pronounced as the leading edge becomes sharp. As a result, the net heat flux to the body surface is reduced. Despite the fact that the number of molecules colliding with the surface by unit time and unit area diminishes with decreasing α_n (see Fig. 4), this tendency is expected because the molecules reflected from the body surface have a higher kinetic energy with the incomplete accommodation model.

The influence of the tangential accommodation coefficient σ_t on the heat transfer coefficient C_h is displayed in Fig. 7. It may be recognized that the heat transfer coefficient exhibits an opposite behavior when compared to that presented by changes in the normal accommodation coefficient, i.e., the heat transfer coefficient increases in the vicinity of the stagnation region with decreasing the tangential accommodation coefficient for the power law shapes investigated. Again, by examining the contribution of the incident q_i and reflected q_r heat fluxes, it is found[5] that both heat fluxes increase slightly close to the stagnation region with diminishing the tangential accommodation coefficient. However, a larger contribution is observed in the incident heat flux, resulting in higher net heat flux.

Pressure Coefficient

The pressure coefficient C_p is defined as follows,

$$C_p = \frac{p_w - p_\infty}{\rho_\infty V_\infty^2/2} \tag{7}$$

where the pressure p_w on the body surface is calculated by the sum of the normal momentum fluxes of both incident and reflected molecules at each time step as follows,

$$p_w = p_i + p_r = \sum_{j=1}^{N} \{[m_j c_{\eta j}]_i + [m_j c_{\eta j}]_r\} \tag{8}$$

where c_η is the normal component of the molecular velocity.

The variation of the pressure coefficient C_p caused by changes in the normal accommodation coefficient

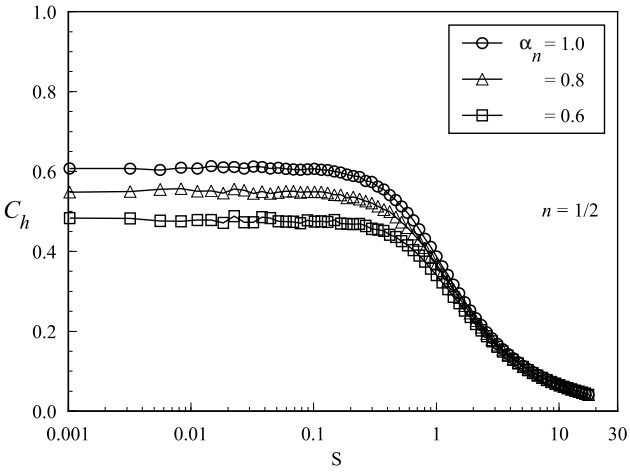

a) $n = 1/2$ **body shape**

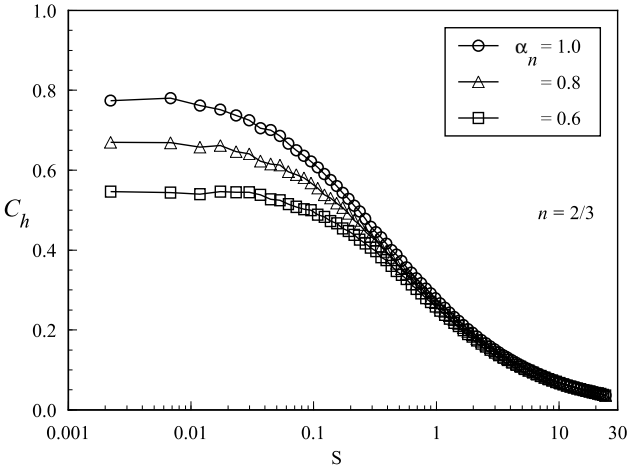

b) $n = 2/3$ **body shape**

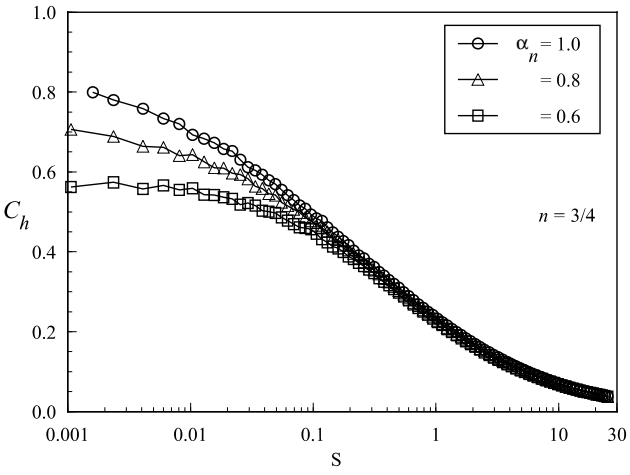

c) $n = 3/4$ **body shape**

Fig. 6 Effect of normal accommodation coefficient α_n on heat transfer coefficient along the body surface.

α_n is demonstrated in Fig. 8 for power law exponents of 1/2, 2/3 and 3/4. It can be seen from this set of pictures that the pressure coefficient distributions

for the partial accommodation calculations are higher than those for full accommodation (diffuse reflection case). In addition, the pressure coefficient increases

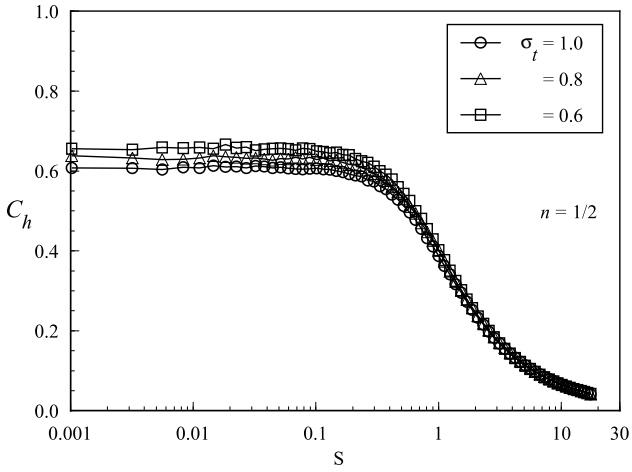

a) $n = 1/2$ **body shape**

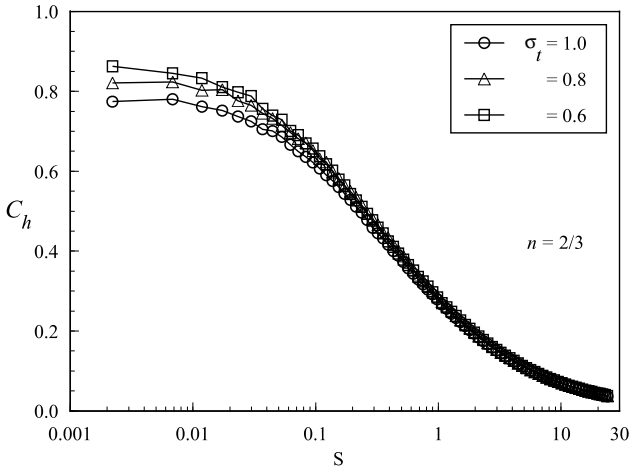

b) $n = 2/3$ **body shape**

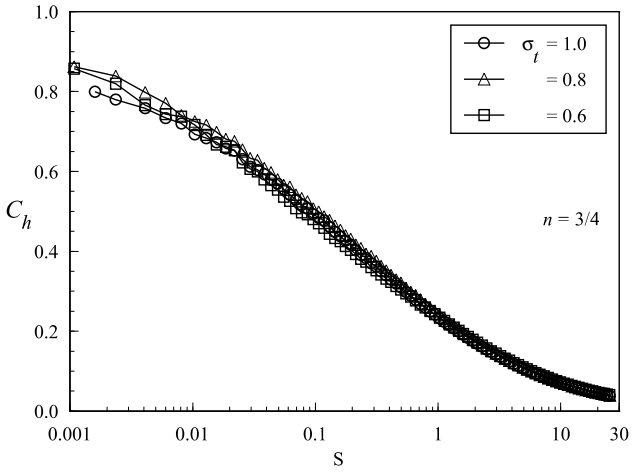

c) $n = 3/4$ **body shape**

Fig. 7 Effect of tangential accommodation coefficient σ_t on heat transfer coefficient along the body surface.

significantly close to the stagnation region as the leading edge shape changes from blunt to sharp. As the accommodation coefficient is reduced from 1.0, the angular distribution of gas molecules reflected from the body surface becomes lobate (see Fig. 1), with preferred scattering tending toward specular reflection. In this context, the shape of the leading edge in the stagnation region plays the important role, since the backward scattering pattern differs substantially from blunt to sharp leading edges. Furthermore, a decrease in the normal accommodation coefficient α_n corresponds to an increase in the reflected component of the normal momentum flux p_r. One way to visualize this behavior is to examine the individual components of the pressure acting on the body surface as defined in Eq.(8). It is noticed[5] that the reflected component of the normal momentum flux p_r increases significantly as α_n decreases from 1.0 to 0.6. In contrast, the incident normal momentum flux p_i decreases slightly for the same range of α_n.

Skin Friction Coefficient

The skin friction coefficient C_f is defined as follows,

$$C_f = \frac{\tau_w}{\rho_\infty V_\infty^2/2} \tag{9}$$

where the shear stress τ_w on the body surface is calculated by the sum of the tangential momentum fluxes of both incident and reflected molecules impinging on the surface at each time step by the following expression,

$$\tau_w = \tau_i + \tau_r = \sum_{j=1}^{N} \{[m_j c_{\xi j}]_i + [m_j c_{\xi j}]_r\} \tag{10}$$

where c_ξ is the tangential component of the molecular velocity.

It is worthwhile to note that for the special case of diffuse reflection, α_n and σ_t equal to 1, the reflected molecules have a tangential moment equal to zero, since the molecules essentially lose, on average, their tangential velocity components. In this fashion, the contribution of the reflected tangential momentum flux τ_r that appears in Eq.(10) is equal to zero. Nevertheless, for incomplete surface accommodation, the reflected tangential momentum flux τ_r contributes to the skin friction coefficient.

The dependence of the skin friction coefficient C_f attributed to variations on the tangential accommodation coefficient σ_t is depicted in Fig. 9. It is immediately evident from Fig. 9 that the change in the tangential accommodation coefficient from σ_t equal to 1.0 to a value of 0.6 produces substantial differences in the magnitude of the skin friction coefficient, particularly in a region of the body surface that corresponds to a body slope angle around of 45 deg[5]. The direction of change is toward lower skin friction coefficient as the accommodation coefficient becomes more incomplete. It is apparent that the major influence on the

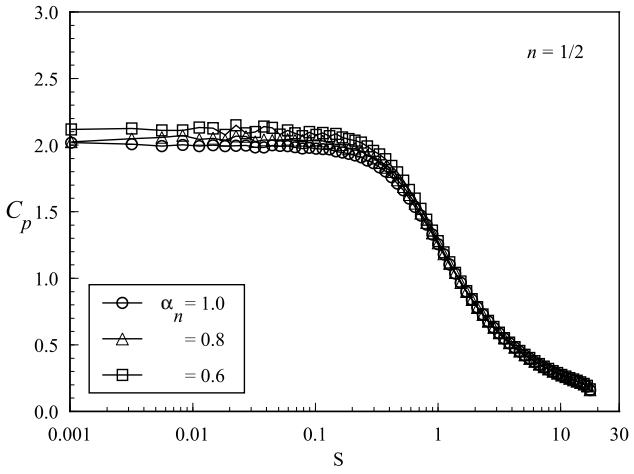

a) $n = 1/2$ **body shape**

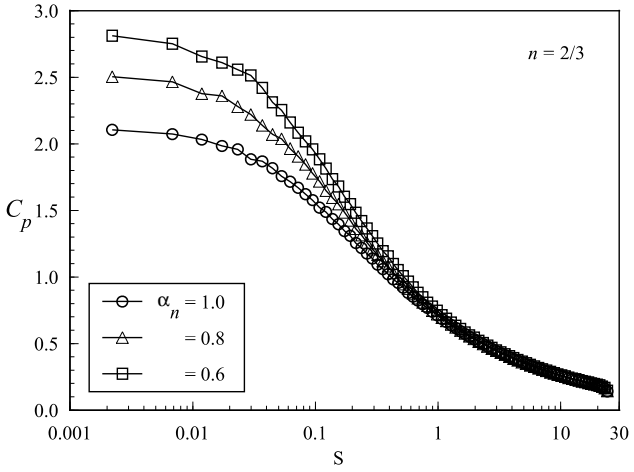

b) $n = 2/3$ **body shape**

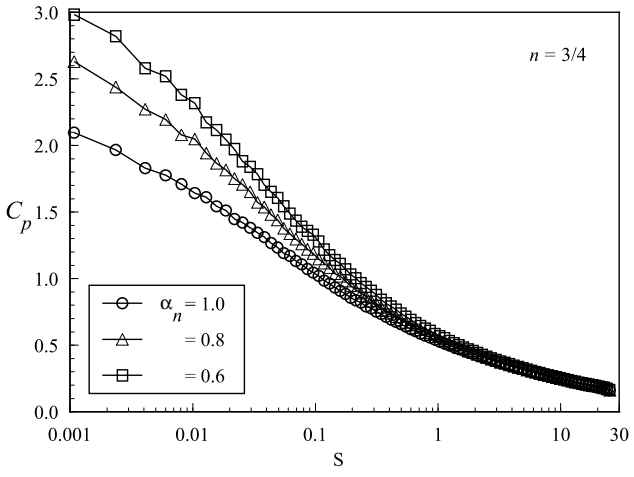

c) $n = 3/4$ **body shape**

Fig. 8 Effect of normal accommodation coefficient α_n on pressure coefficient along the body surface.

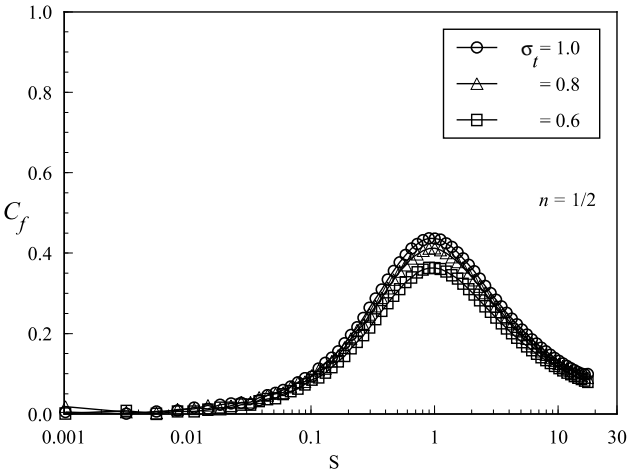

a) $n = 1/2$ **body shape**

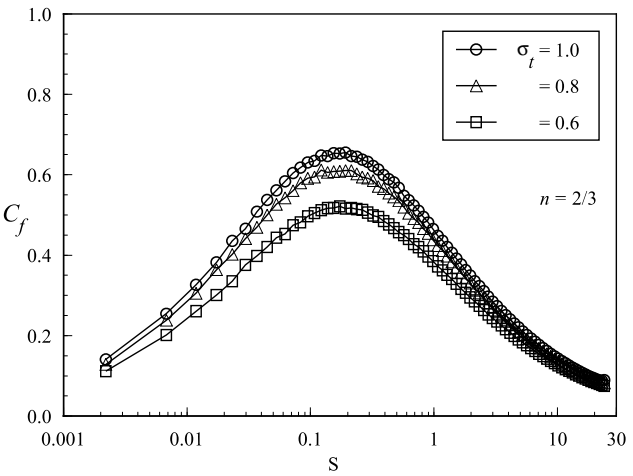

b) $n = 2/3$ **body shape**

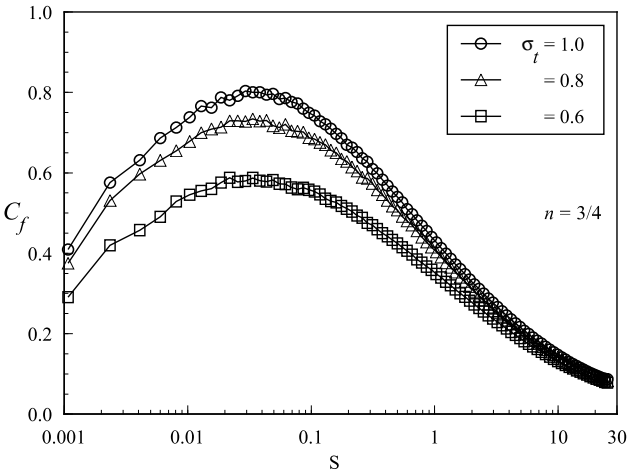

c) $n = 3/4$ **body shape**

Fig. 9 Effect of tangential accommodation coefficient σ_t on skin friction coefficient along the body surface.

skin friction coefficient comes from the contribution of the reflected momentum flux of the molecules that increases significantly with decreasing σ_t.

Total Drag Coefficient

The total drag coefficient is defined as being,

$$C_d = \frac{D}{\rho_\infty V_\infty^2 H/2} \tag{11}$$

where D is the resultant force acting on the body surface, and H is the height at the matching point common to the leading edges (see Fig. 2).

The resultant force acting on the body surface was obtained by the integration of the pressure p_w and shear stress τ_w distributions from the stagnation point of the leading edges to the station L that corresponds to the tangential point common to all shapes. It is worthwhile to mention that the values for the total drag coefficient were obtained by assuming the shapes acting as leading edges. As a result, no base pressure effects were taken into account on the calculations.

The extent of the changes in the total drag coefficient C_d with decreasing the normal and tangential accommodation coefficients is illustrated in Fig. 10 for power law exponents of 1/2, 2/3 and 3/4. Referring to Fig. 10, it can be seen that the total drag coefficient increases by a reduction in the normal accommodation coefficient, and decreases by a reduction in the tangential accommodation coefficient. The major contribution to the drag coefficient rise is attributed to the pressure coefficient, which increases with decreasing α_n, as shown in Fig. 8. In contrast, the major contribution to the drag coefficient reduction is attributed to the skin friction coefficient, which diminishes with decreasing σ_t, as illustrated in Fig. 9.

Concluding Remarks

This study applies the Direct Simulation Monte Carlo method to investigate rarefied gas over power law shaped leading edges. Effects of incomplete surface accommodation on the heat transfer, pressure, skin friction, and drag coefficients for a representative range of normal and tangential accommodation coefficients are investigated. The normal and tangential accommodation coefficients are varied from 1.0 to 0.6, and the power law exponent ranges from 1/2 to 3/4. Cases considered in this study cover the hypersonic flow on the transitional regime.

Calculations showed that a reduction in the normal accommodation coefficient from 1.0 to 0.6 decreased the heat transfer coefficient in the vicinity of the stagnation point for the power law shapes investigated. In contrast, a reduction in the tangential accommodation coefficient increased slightly the heat transfer coefficient near the nose of the leading edges. Also, it was found that the total drag coefficient is reduced by a reduction in the tangential accommodation coefficient, and increased by a reduction in the normal accommodation coefficient.

The effects of either normal or tangential accommodation coefficient showed that in order to make accurate predictions of the aerodynamic forces on, and heat transfer rates to, bodies in rarefied hypersonic flow it will be necessary to take surface accommodation into account.

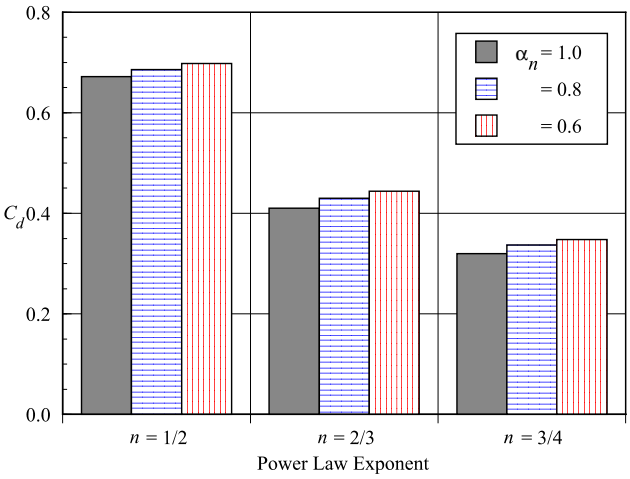

a) Normal accommodation coefficient

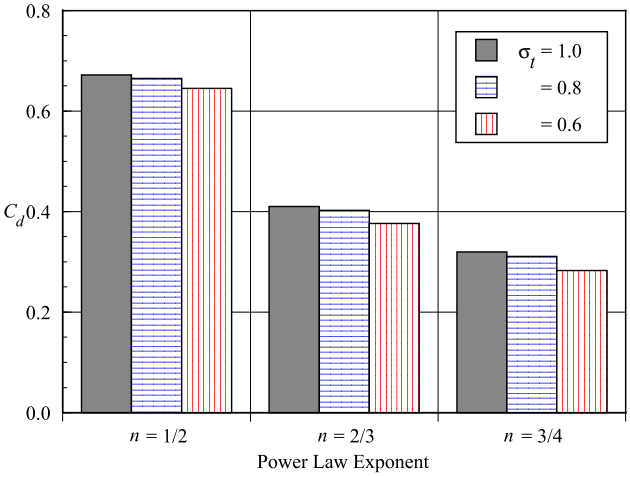

b) Tangential accommodation coefficient

Fig. 10 Effect of normal and tangential accommodation coefficients on total drag coefficient for power law exponents of 1/2, 2/3 and 3/4.

References

[1] Cercignani, C., *The Boltzmann Equation and Its Applications,* Springer-Verlag, New York, NY, 1988.

[2] Bird, G. A., *Molecular Gas Dynamics and the Direct Simulation of Gas Flows*, Oxford University Press, Oxford, England, UK, 1994.

[3] Mason, W. H. and Lee, J., "Aerodynamically Blunt and Sharp Bodies," *J. of Spacecraft and Rockets*, vol. 31, No. 3, 1994, pp. 378–382.

[4] O'Brien, T. F. and Lewis, M. J., "Power Law Shapes for Leading-Edge Blunting with Minimal Shock Standoff," *J. of Spacecraft and Rockets*, vol. 36, No. 5, 1999, pp. 653–658.

[5] Santos, W. F. N., "Direct Simulation Monte Carlo of Rarefied Hypersonic Flow on Power Law Shaped Leading Edges," Ph.D. Dissertation, Dept. of Aerospace Engineering, University of

Maryland, College Park, MD, Dec., 2001.

[6] Santos, W. F. N., and Lewis, M. J., "Power Law Shaped Leading Edges in Rarefied Hypersonic Flow," *Journal of Spacecraft and Rockets*, Vol. 39, No. 6, 2002, pp. 917–925.

[7] Santos, W. F. N., and Lewis, M. J., "Angle of Attack Effect on Rarefied Hypersonic Flow over Power Law Shaped Leading Edges," in *23rd International Symposium on Rarefied Gas Dynamics*, Whistler, BC, Canada, July 20-25, 2002.

[8] Santos, W. F. N., and Lewis, M. J., "Shock Wave Structure in a Rarefied Hypersonic Flow on Power Law Shaped Leading Edges," in *41st AIAA Aerospace Sciences Meeting and Exhibit*, AIAA Paper 2003-1134, Reno, NV, January 6-9, 2003.

[9] Santos, W. F. N., and Lewis, M. J., "Aerodynamic Heating Performance of Power Law Leading Edges in Rarefied Hypersonic Flow," in *36th AIAA Thermophysics Conference*, AIAA Paper 2003-3894, Orlando, FL, June 23-26, 2003.

[10] Santos, W. F. N., and Lewis, M. J., "Effects of Compressibility on Rarefied Hypersonic Flow over Power Law Leading Edges," in *42nd AIAA Aerospace Sciences Meeting and Exhibit*, AIAA Paper 2004-1181, Reno, NV, January 5-8, 2004.

[11] Nonweiler, T. R. F., "Aerodynamic Problems of Manned Space Vehicles," *J. of the Royal Aeronautical Society*, Vol. 63, Sept, 1959, pp. 521–528.

[12] Anderson, J. L., "Tethered Aerothermodynamic Research for Hypersonic Waveriders," in *Proceedings of the 1st International Hypersonic Waverider Symposium*, Univ. of Maryland, College Park, MD, 1990.

[13] Potter, J. L. and Rockaway, J. K., "Aerodynamic Optimization for Hypersonic Flight at Very High Altitudes," in *Rarefied gas Dynamics: Space Science and Engineering*, edited by B. D. Shizgal and D. P. Weaver, Vol. 160, Progress in Astronautics and Aeronautics, AIAA New York, 1994, pp. 296–307.

[14] Rault, D. F. G., "Aerodynamic Characteristics of a Hypersonic Viscous Optimized Waverider at High Altitude," *J. of Spacecraft and Rockets*, vol. 31, No. 5, 1994, pp. 719–727.

[15] Graves, R. E. and Argrow, B. M., "Aerodynamic Performance of an Osculating-Cones Waverider at High Altitudes," in *35th AIAA Thermophysics Conference*, AIAA Paper 2001-2960, Anaheim, CA, 2001.

[16] Lord, R. G., "Application of the Cercignani-Lampis Scattering Kernel to Direct Simulation Monte Carlo Method," in *17th International Symposium on Rarefied Gas Dynamics*, edited by A. E. Beylich, Aachen, Germany, pp. 1427-1433, July 8-14, 1991.

[17] Schaaf, S. A. and Chambre, P. L., *Flow of Rarefied Gases,* Princeton Aeronautical Paperbacks, Princeton University Press, Princeton, NJ, 1961.

[18] Cercignani, C. and Lampis, M., "Kinetic Models for Gas-Surface Interactions," *Transport Theory and Statistical Physics*, Vol. 1, No. 2, 1971, pp. 101–114.

[19] Lord, R. G., "Some Extensions to the Cercignani-Lampis Gas-Surface Scattering Kernel," *Physics of Fluids*, Vol. A3, No. 4, 1991, pp. 706–710.

[20] Lord, R. G., "Some Further Extensions of the Cercignani-Lampis Gas-Surface Interaction Model," *Physics of Fluids*, Vol. 7, No. 5, 1995, pp. 1159–1161.

[21] Bird, G. A., "Monte Carlo Simulation in an Engineering Context," in *Progress in Astronautics and Aeronautics: Rarefied gas Dynamics*, edited by Sam S. Fisher, Vol. 74, part I, AIAA New York, 1981, pp. 239–255.

[22] Bird, G. A., "Perception of Numerical Method in Rarefied Gasdynamics," in *Rarefied gas Dynamics: Theoretical and Computational Techniques*, edited by E. P. Muntz, and D. P. Weaver and D. H. Campbell, Vol. 118, Progress in Astronautics and Aeronautics, AIAA, New York, 1989, pp. 374–395.

[23] Borgnakke, C. and Larsen, P. S., "Statistical Collision Model for Monte Carlo Simulation of Polyatomic Gas Mixture," *Journal of computational Physics*, vol. 18, No. 4, 1975, pp. 405–420.

[24] Alexander, F. J., Garcia, A. L., and, Alder, B. J., "Cell Size Dependence of Transport Coefficient is Stochastic Particle Algorithms," *Physics of Fluids*, Vol. 10, No. 6, 1998, pp. 1540–1542.

[25] Alexander, F. J., Garcia, A. L., and, Alder, B. J., "Erratum: Cell Size Dependence of Transport Coefficient is Stochastic Particle Algorithms," *Physics of Fluids*, Vol. 12, No. 3, 2000, pp. 731–731.

[26] Garcia, A. L., and, Wagner, W., "Time Step Truncation Error in Direct Simulation Monte Carlo," *Physics of Fluids*, Vol. 12, No. 10, 2000, pp. 2621–2633.

[27] Hadjiconstantinou, N. G., "Analysis of Discretization in the Direct Simulation Monte Carlo," *Physics of Fluids*, Vol. 12, No. 10, 2000, pp. 2634–2638.